CHEMSUSCHEM

ChemPubSoc Europe

DOI: 10.1002/cssc.201200286

1D Coaxial Platinum/Titanium Nitride Nanotube Arrays with Enhanced Electrocatalytic Activity for the Oxygen Reduction Reaction: Towards Li–Air Batteries

Shanmu Dong,[a] Xiao Chen,[a] Shan Wang,[a] Lin Gu,[b] Lixue Zhang,[a] Xiaogang Wang,[a] Xinhong Zhou,[c] Zhihong Liu,[a] Pengxian Han,[a] Yulong Duan,[a] Hongxia Xu,[a] Jianhua Yao,[a] Chuanjian Zhang,[a] Kejun Zhang,[a] Guanglei Cui,*[a] and Liquan Chen[b]

The electrocatalytic reduction of oxygen is a key reaction for converting chemical energy to electrical energy in fuel cells and lithium–air (oxygen) batteries.[1–4] The most efficient oxygen reduction reaction (ORR) electrocatalysts reported so far are platinum-based materials.[5–9] However, the high costs and limited resources of platinum pose ever-increasing challenges to the development of such electrocatalysts.[10] The most commonly used strategy to minimize the amount of platinum, and thus enhance the specific activity, involves the use of conductive carbon materials with high surface areas as supports for the dispersion of platinum nanoparticles.[11–16] However, recent studies have revealed that the effective use of platinum electrocatalysts not only depends on the intrinsic catalytic activity of platinum but also strongly on the characteristics of the catalyst support, and hence much effort has been devoted to the development of new catalyst supports to further enhance the electrocatalytic performance of platinum-based catalysts.[17–20]

An ideal catalyst support should have a low combustive reactivity, superior electrochemical stability, and good electronic conductivity.[21,22] In addition, interactions between platinum and the support material should be taken into account because suitable supports can reduce the binding of –OH on the surface of the platinum catalyst and hence facilitate O_2 adsorption and activation.[23,24] Among the various choices of support material, titanium nitride is a promising candidate because it offers a good corrosion resistance, low cost, and excellent electronic conductivity.[25–27] The morphology of titanium nitride materials can be readily tuned, which is favorable for the loading of catalysts.[28–32] Furthermore, titanium may act as a center for the adsorption of –OH and decrease the coverage of platinum by –OH, resulting in an increased adsorption of O_2 onto the platinum surface and enhanced ORR activity.[33–36] However, the number of reports on the use of titanium nitride as catalyst support is still limited.

In this study, we propose a new electrode motif by integrating the favorable features of vertically aligned titanium nitride nanotube arrays (TiN NTA) and a platinum catalyst electrodeposited into the TiN NTA's coaxial nanotube arrays. The nanotube-like structure of the platinum layer offers a superior stability,[37–41] while the TiN NTA support is favorable for electron-transfer and the diffusion of reactant gases. In our previous work, TiN NTA proved an effective current collector for supercapacitor applications,[42] and hence the material is expected to be an ideal support for electrocatalysis. Herein, a 1D Pt/TiN coaxial nanotube array (Pt/TiN NTA) is prepared by electrodepositing platinum into TiN NTA, which in turn is fabricated by the anodization of a titanium foil substrate and subsequent nitridation using ammonia annealing.[32] The nanostructured Pt/TiN NTA is used to study the ORR and consequently explored as O_2 cathode in an aprotic/aqueous hybrid electrolyte Li–air battery.

The fabrication of vertically aligned TiN NTA was described in our previous report.[42] Electrodeposition was employed to uniformly load the platinum layer along the nanotube wall because this technique is favorable for morphology control by tuning of the applied potential and electrolyte ingredients (Figure 1a).[42,43] As determined by comparing scanning electron microscopy (SEM) images of bare TiN NTA (Figure 1b, inset) and the sample after electrodeposition (Figure 1b and c), a thin layer of platinum (20–25 nm) was evenly deposited along the walls of the titanium nitride nanotubes, forming a nanotube-like structure. Low-magnification transmission electron microscopy (TEM) images (Figure 1d) also clearly reveal the coaxial nanotube morphology. As revealed by higher-magnification TEM images (Figure 1d, upper left inset) the deposited platinum layer is highly porous, endowing the 1D nanostructured materials with a large surface area. Furthermore, energy dispersive X-ray spectroscopy (EDX) measurements confirmed the presence of platinum in the nanostructure (Figure 2a). An inductively coupled plasma (ICP) analysis of a solution of platinum from dissolved Pt/TiN NTA indicated that 8 μg of platinum had been loaded on the TiN NTA (0.25 cm^2). This coaxial 1D motif provides an enhanced contact between the platinum layer and the conductive titanium nitride support, which is highly advantageous for the ORR.[18,40,44,45]

[a] S. Dong,[+] Dr. X. Chen,[+] S. Wang, Dr. L. Zhang, X. Wang, Dr. Z. Liu, P. Han, Y. Duan, Dr. H. Xu, J. Yao, C. Zhang, K. Zhang, Prof. G. Cui
Biomimetics Energy Group
Qingdao Institute of Bioenergy and Bioprocess Technology
Chinese Academy of Sciences
Qingdao 266101 (PR China)
Fax: (+86) 532-80662746
E-mail: cuigl@qibebt.ac.cn

[b] L. Gu, Prof. L. Chen
Beijing National Laboratory for Condensed Matter Physics
Institute of Physics, Chinese Academy of Sciences
Beijing 100080 (PR China)

[c] Dr. X. Zhou
College of Chemistry and Molecular Engineering
Qingdao University of Science and Technology
Qingdao 266101 (PR China)

[+] These authors contributed equally to this work.

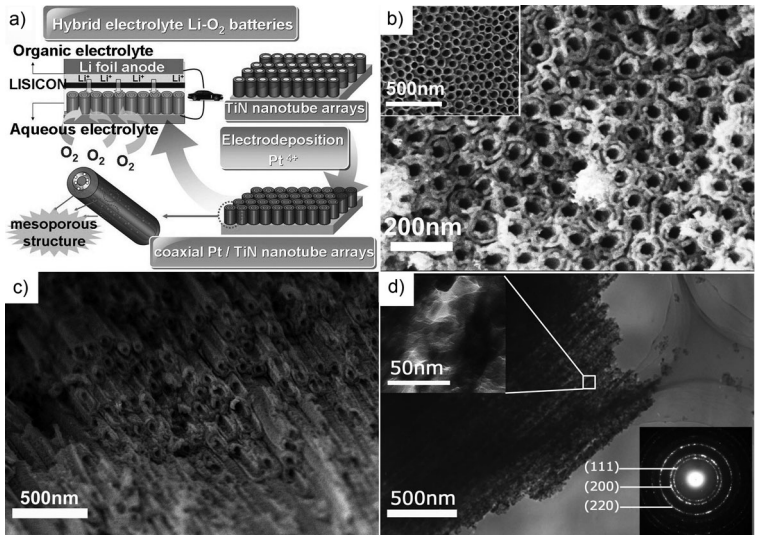

Figure 1. a) Schematic of the preparation of Pt/TiN NTA and the structure of the Li–air batteries. b) Top-view FESEM images of Pt/TiN NTA and TiN NTA (inset). c) Cross-sectional FESEM image of Pt/TiN NTA (mechanically fractured). d) Low- and high-magnification (upper left inset) TEM images of Pt/TiN NTA and SAED patterns of the platinum layer (lower right inset).

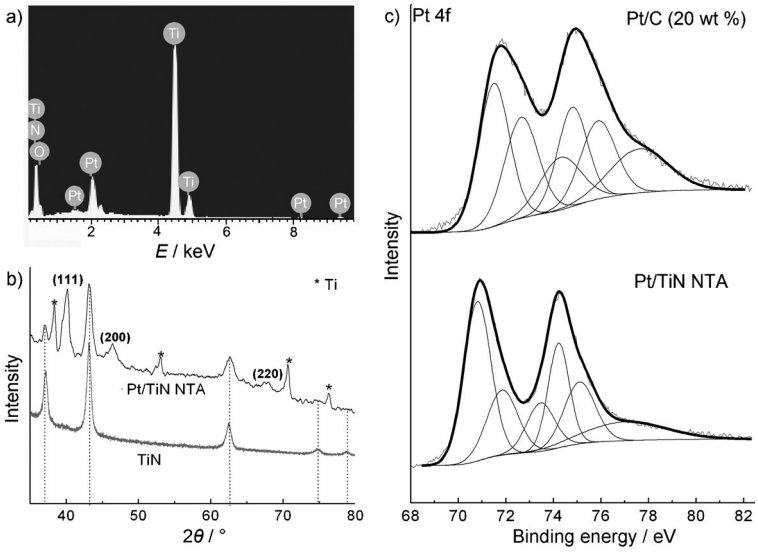

Figure 2. a) EDX spectrum patterns of Pt/TiN NTA. b) XRD patterns of TiN and Pt/TiN NTA (the peaks marked by asterisks originate from the titanium foil substrate. c) Pt 4f XPS spectra of Pt/TiN NTA and commercial Pt/C (20 wt% Pt).

An X-ray diffraction (XRD) pattern of the Pt/TiN NTA sample is shown in Figure 2b. Compared to the pattern of titanium nitride, peaks at 40.0°, 46.4°, and 67.6° can be assigned to (111), (200), and (220) reflections of face-centered cubic (fcc) platinum (space group: Fm3m), which suggests that the electrodeposited platinum is of crystalline nature. This result is further confirmed by selected-area electron diffraction (SAED) patterns (Figure 1d, lower right inset) that show continuous rings and discrete diffraction spots, indicating that the primary particles are highly crystalline.

X-ray photoelectron spectroscopy (XPS) was used to probe the interaction between platinum and the TiN NTA support. Figure 2c shows the Pt 4f spectrum of Pt/TiN NTA. The spectrum was deconvoluted into three pairs of doublets, ascribed to metallic Pt, Pt^{2+}, and Pt^{4+}.[46] The most intense doublet, with a binding energy of 70.8 eV (Pt $4f_{7/2}$) and 74.5 eV (Pt $4f_{5/2}$) was attributed to Pt^0, in good agreement with the value of bulk Pt. By contrast, the same peaks of commercial Pt/C (20 wt% Pt, JM Co.) obviously shifted to a high binding energy. According to a previous report, this is due to small cluster-size effects on carbon supports.[46,47] Notably, the relative intensity of Pt^0 in Pt/TiN NTA is higher than in Pt/C, which indicates a lower oxidation state of platinum on TiN NTA.[46,48] This might results from a transfer of electronic charge, from the titanium-based support to the platinum clusters.[35,36] Because a lower oxidation state of platinum on the catalyst surface is believed to improve activity towards the ORR,[46,48] the Pt/TiN NTA nanostructure can be expected to deliver superior electrocatalytic activity.

Inspired by these attractive properties, the electrocatalytic performance of the Pt/TiN NTA electrode towards the cathodic ORR was evaluated by using cyclic voltammetry (CV). The Pt/C (20 wt%) catalyst was tested for comparison. CV curves recorded between 0.2 and −0.6 V vs. Ag/AgCl in an aqueous solution of 1 M $LiNO_3$ + 0.5 M LiOH are shown in Figure 3a. Only background currents, representing electrode characteristics, are observed in the argon-saturated solution, which can be mainly attributed to the double layer capacitive current of TiN NTA.[49] In contrast, the CV curve clearly showed an oxygen reduction current when the solution was saturated with O_2. By subtracting the capacitive current measured under argon (Figure 3c), a well-defined cathodic peak could be demarcated at −0.13 V, with an onset potential of −0.01 V. The electrochemical active surface areas (ECSAs) of the samples were calculated by integrating the charge passed during the hydrogen desorption from the electrode surface after capacity correction.[50] The ECSA obtained for Pt/TiN NTA was 35.9 $m^2 g_{Pt}^{-1}$, which is comparable to that for the commercial Pt/C catalyst: 28.0 $m^2 g_{Pt}^{-1}$.[37,38,41] The ORR electrocatalytic activities of the Pt/TiN NTA and commercial Pt/C catalysts are shown in Figure 3c. Both linear sweep voltammetry curves were obtained in an O_2-saturated aqueous solution after capacity correction. The Pt/TiN NTA displayed a more positive onset potential and higher mass activity (2.1 times) towards the ORR than the Pt/C catalyst (Figure 3d). Taking into account the ECSA of platinum, the specific activity of Pt/TiN NTA is still 1.6 times higher than that of commercial Pt/C. The enhanced electrocatalytic activity of the Pt/TiN NTA material can be attributed to several factors. Firstly, the unique 1D coaxial nanostructure enables preferential exposure of certain crystal facets of the platinum material and facilitates electron transport and gas diffusion by the TiN NTA framework.[17] Secondly, the lower oxidation state of platinum on the surface of Pt/TiN NTA, indicating a favorable interaction between platinum and the titanium nitride support,

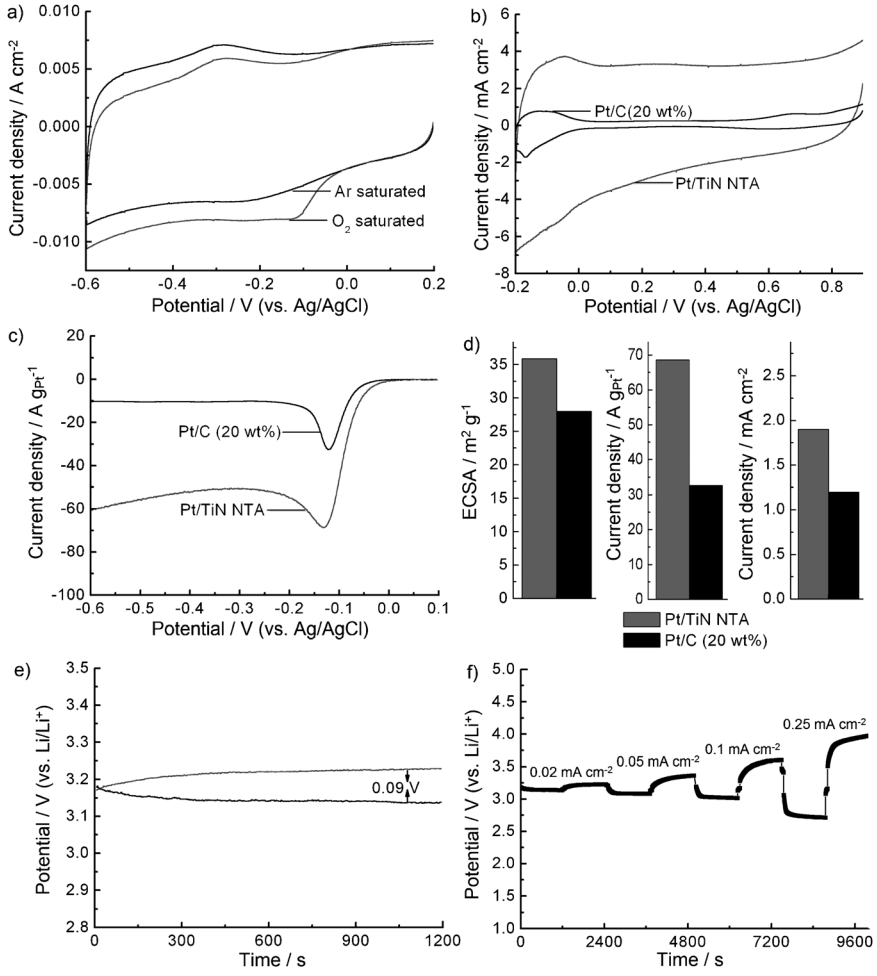

Figure 3. a) CV curves of Pt/TiN NTA in aqueous electrolyte of 1 M $LiNO_3$ + 0.5 M LiOH solution at a scan rate of 20 mV s^{-1}, in the presence and absence of O_2. b) CV curves of Pt/TiN NTA and commercial Pt/C (20 wt% Pt) in an argon-saturated 0.5 M H_2SO_4 solution at a scan rate of 20 mV s^{-1}. c) LSV curves of Pt/TiN NTA and commercial Pt/C (20 wt.% Pt) in an O_2-saturated electrolyte of 1 M $LiNO_3$ + 0.5 M LiOH with a scan rate of 20 mV s^{-1}. d) Electrochemical surface area activity (ECSA, $m^2 g^{-1}$), the mass activity (A mg^{-1}, at −0.13 V), and the specific activity (mA cm^{-2} Pt, at −0.13 V) of Pt/TiN NTA, compared to commercial Pt/C (20 wt% Pt). e) Charge–discharge curves of a Pt/TiN NTA cathode-based Li–air cell at 0.02 mA cm^{-2}, using lithium disk as anode, 1 M $LiPF_6$ in EC/DMC as the organic electrolyte, and 1 M $LiNO_3$ + 0.5 M LiOH solution as the aqueous electrolyte. A LISICON film is used to separate the organic and aqueous electrolytes. f) Charge–discharge curves of Pt/TiN NTA cathode based Li–air cell at different current densities

may enhance the specific activity.[46,48] Finally, the presence of titanium on the support may reduce the coverage of platinum by –OH, further improving the catalytic activity.[35,36]

Furthermore, the performance of the Pt/TiN NTA material as cathode in a Li–air battery with an aprotic/aqueous hybrid electrolyte was tested. In this system, LiOH is formed via ORR during the discharging process and undergoes an O_2 evolution reaction during the charging process. Charge–discharge curves of the Li–air battery are given in Figure 3e. The gap between the discharge and charge plateaus is only 0.09 V (Figure 3d, inset) at 0.02 mA cm^{-2}, demonstrating the low overpotential characteristic of the Pt/TiN NTA cathode. At current densities higher than 0.05 mA cm^{-2}, a voltage gap and the simultaneous disappearance of the flat charge plateaus are gradually becoming apparent (Figure 3f). This may be caused by the inadequate ionic conductivity of LISICON at higher current densities and inadequate O_2 supplement in the aqueous solution.[51,52] These preliminary results are not yet optimized in terms of cycle life. However, the 1D coaxial Pt/TiN NTA indeed exhibit a promising electrocatalytic activity towards ORR, offering an attractive option for oxygen cathodes in Li-air batteries.

In summary, a well-designed 1D coaxial Pt/TiN NTA material is successfully prepared by electrodeposition of platinum into a titanium nitride nanotube array. Compared to a commercial Pt/C catalyst (with 20 wt% Pt), the Pt/TiN NTA electrode exhibits superior mass activity (2.1 times) and specific activity (1.6 times). The superior catalytic activity can be attributed to the TiN NTA support, which offers a combination of advantageous characteristic compared to carbon supports: (i) the unique structural and conductivity features of the NTA structure, (ii) a lower oxidation state of platinum due to favorable interactions with the catalytic metal, and (iii) reduced coverage of platinum by –OH due to the presence of titanium in the support. Furthermore, the Pt/TiN NTA material is used as cathode in a hybrid electrolyte Li–air battery. This cathode exhibits a low potential gap of 0.09 V between the charge and discharge curves at 0.02 mA cm^{-2}, indicating that coaxial Pt/TiN NTA is a promising cathode for aprotic/aqueous hybrid electrolyte Li–air batteries. Furthermore, TiN NTA-based coaxial nanostructures can offer a platform for the design of electrode materials for fuel cells, metal–air batteries, and biosensors.

Experimental Section

Titanium nitride nanotube arrays were prepared as described in a previous report.[32] Electrodeposition was done by using a CHI440a electrochemical workstation (CHI Instrument Inc.) at room temperature with a three-electrode cell consisting of a Ag/AgCl electrode as reference electrode, a 10 × 10 mm platinum plate as counter electrode, and TiN NTA/Ti foil (25 mm^2) as working electrode. In a typical procedure, coaxial Pt/TiN nanotube arrays were fabricated by using a potentiostat at −0.5 V (vs. Ag/AgCl) in an aqueous solution of 2.5 mM H_2PtCl_6 ($H_2PtCl_6 \cdot 6H_2O$, Shanghai Chemical Reagent Co.) and 0.1 M HCl (Shanghai Chemical Reagent Co.)

for 100 s. After deposition, the coaxial nanostructured arrays were thoroughly rinsed with distilled water and ethanol to remove soluble material. The as-prepared samples were subsequently dried at 50 °C overnight.

X-ray diffraction (XRD) measurements of Pt/TiN NTA were recorded in a Bruker-AXS Micro-diffractometer (D8 ADVANCE) from 10° to 85°. X-ray photoelectron spectroscopy (XPS) data was obtained with an ESCALab220i-XL electron spectrometer from VG Scientific using AlK_α radiation. ICP measurements were carried out by Terracon (GmbH & Co. KG). The morphology of the Pt/TiN NTA was attained from field emission scanning electron microscopy (FESEM, HITACHI S-4800) and high-resolution transmission electron microscopy (HR-TEM, JEOL 2010F).

The structure of the hybrid electrolyte Li–air battery is shown in Figure 1a, 1 M $LiPF_6$ in EC/DMC (EC/DMC = 1:1) as the electrolyte for the Li anode and 1 M $LiNO_3$ + 0.5 M LiOH was used as the aqueous electrolyte. $Li_{1+x+y}Al_x(Ti, Ge)_{2-x}Si_yP_{3-y}O_{12}$ (LISICON, Ohara) was used as a solid-state electrolyte film (0.25 mm thick) to separate the organic and aqueous electrolytes. A glass-fiber separator was put between the lithium foil and the solid electrolyte to avoid reduction of the LISICON by direct contact with the anode. The battery was assembled in an argon-filled glove box. The galvanostatical discharge-charge experiments were carried out with a LAND battery testing system and the cyclic voltametry (CV) and linear sweep voltammetry (LSV) tests of the electrodes were carried out via an electrochemical workstation (CHI440a, CHI Instrument Inc.).

Acknowledgements

This work was supported by the Key Research Program of the Chinese Academy of Sciences (KGZD-EW-202-2), the National Program on Key Basic Research Project of China (973 Program) (MOST2011CB935700), the "100 Talents" program of the Chinese Academy of Sciences, Shangdong Province Fund for Distinguished Young Scientist (JQ200906), the National Natural Science Foundation (20971077, 20901044, and 20902052).

Keywords: batteries · lithium · nanostructures · nitrides · platinum

[1] G. Wu, K. L. More, C. M. Johnston, P. Zelenay, *Science* **2011**, *332*, 443.
[2] E. Yoo, H. Zhou, *ACS Nano* **2011**, *5*, 3020.
[3] M. Lefèvre, E. Proietti, F. Jaouen, J. P. Dodelet, *Science* **2009**, *324*, 71.
[4] M. Zhang, Y. Yan, K. Gong, L. Mao, Z. Guo, Y. Chen, *Langmuir* **2004**, *20*, 8781.
[5] K. Kinoshita, *Electrochemical Oxygen Technology*, Wiley, New York, **1992**.
[6] H. A. Gasteiger, N. M. Marković, *Science* **2009**, *324*, 48.
[7] S. Wang, S. P. Jiang, T. J. White, J. Guo, X. Wang, *J. Phys. Chem. C* **2009**, *113*, 18935.
[8] H. Yano, J. M. Song, H. Uchida, M. Watanabe, *J. Phys. Chem. C* **2008**, *112*, 8372.
[9] D. J. Guo, X. P. Qiu, L. Q. Chen, W. T. Zhu, *Carbon* **2009**, *47*, 1680.
[10] S. Wang, D. Yu, L. Dai, *J. Am. Chem. Soc.* **2011**, *133*, 5182.
[11] Z. Liu, X. Ling, X. Su, J. Lee, *J. Phys. Chem. B* **2004**, *108*, 8234.
[12] Z. Zhou, S. Wang, W. Zhou, G. Wang, L. Jiang, W. Li, S. Song, J. Liu, G. Sun, Q. Xin, *Chem. Commun.* **2003**, 394.
[13] C. K. Poh, S. H. Lim, H. Pan, J. Lin, J. Y. Lee, *J. Power Sources* **2008**, *176*, 70.
[14] K. I. Han, J. S. Lee, S. O. Park, S. W. Lee, Y. W. Park, H. Kim, *Electrochim. Acta* **2004**, *50*, 791.
[15] S. H. Joo, S. J. Choi, I. Oh, J. Kwak, Z. Liu, O. Terasaki, R. Ryoo, *Nature* **2001**, *412*, 169.
[16] J. S. Guo, G. Q. Sun, Q. Wang, G. X. Wang, Z. H. Zhou, S. H. Tang, L. H. Jiang, B. Zhou, Q. Xin, *Carbon* **2006**, *44*, 152.
[17] Z. Q. Tian, S. H. Lim, C. K. Poh, Z. Tang, Z. Xia, Z. Luo, P. K. Shen, D. Chua, Y. P. Feng, Z. Shen, J. Lin, *Adv. Energy Mater.* **2011**, *1*, 1205.
[18] S. Chen, Z. Wei, L. Guo, W. Ding, L. Dong, P. Shen, X. Qia, L. Lia, *Chem. Commun.* **2011**, *47*, 10984.
[19] Y. Liu, J. Chen, W. Zhang, Z. Ma, G. F. Swiegers, C. O. Too, G. G. Wallace, *Chem. Mater.* **2008**, *20*, 2603.
[20] J. Masa, A. Bordoloi, M. Muhler, W. Schuhmann, W. Xia, *ChemSusChem* **2012**, *5*, 523.
[21] Y. Shao, J. Liu, Y. Wang, Y. Lin, *J. Mater. Chem.* **2009**, *19*, 46.
[22] A. Morozan, B. Jousselme, S. Palacin, *Energy Environ. Sci.* **2011**, *4*, 1238.
[23] C. C. Liang, A. L. Juliard, *J. Electroanal. Chem.* **1965**, *9*, 390.
[24] T. Toda, H. Igarashi, H. Uchida, M. Watanabe, *J. Electrochem. Soc.* **1999**, *146*, 3750.
[25] O. T. M. Musthafa, S. Sampath, *Chem. Commun.* **2008**, 67.
[26] Z. Wen, S. Cui, H. Pu, S. Mao, K. Yu, X. Feng, J. Chen, *Adv. Mater.* **2011**, *23*, 544.
[27] J. Chen, K. Takanabe, R. Ohnishi, D. Lu, S. Okada, H. Hatasawa, H. Morioka, M. Antonietti, J. Kubota, K. Domen, *Chem. Commun.* **2010**, *46*, 7492.
[28] A. Fischer, P. Makowski, J. O. Muller, M. Antonietti, A. Thomas, F. Goettmann, *ChemSusChem* **2008**, *1*, 444.
[29] W. Yao, P. Makowski, C. Giordano, F. Goettmann, *Chem. Eur. J.* **2009**, *15*, 11999.
[30] Y. Jun, W. H. Hong, M. Antonietti, A. Thomas, *Adv. Mater.* **2009**, *21*, 4270.
[31] K. Bang, S. Suslick, *Adv. Mater.* **2009**, *21*, 3186.
[32] Q. W. Jiang, G. R. Li, X. P. Gao, *Chem. Commun.* **2009**, 6720 – 6722.
[33] J. Zhang, M. B. Vukmirovic, K. Sasaki, A. U. Nilekar, M. Mavrikakis, R. R. Adzic, *J. Am. Chem. Soc.* **2005**, *127*, 12480.
[34] M. B. Vukmirovic, J. Zhang, K. Sasaki, A. U. Nilekar, F. Uribe, M. Mavrikakis, R. R. Adzic, *Electrochim. Acta* **2007**, *52*, 2257.
[35] K. D. Schierbaum, S. Fischer, M. C. Torquemada, J. L. de Segovia, E. Romam, J. A. Martin-Gago, *Surf. Sci.* **1996**, *345*, 261.
[36] J.-M. Chen, L. S. Sarma, C.-H. Chen, M.-Y. Cheng, S.-C. Shih, G.-R. Wang, D.-G. Liu, J.-F. Lee, M.-T. Tang, B.-J. Hwang, *J. Power Sources* **2006**, *159*, 29.
[37] H.-W. Liang, X. Cao, F. Zhou, C.-H. Cui, W.-J. Zhang, S.-H. Yu, *Adv. Mater.* **2011**, *23*, 1467.
[38] S. Sun, G. Zhang, D. Geng, Y. Chen, M. N. Banis, R. Li, M. Cai, X. Sun, *Chem. Eur. J.* **2010**, *16*, 829.
[39] C. Xu, L. Wang, R. Wang, K. Wang, Y. Zhang, F. Tian, Y. Ding, *Adv. Mater.* **2009**, *21*, 2165.
[40] C. Koenigsmann, A. C. Santulli, K. Gong, M. B. Vukmirovic, W.-P. Zhou, E. Sutter, S. S. Wong, R. R. Adzic, *J. Am. Chem. Soc.* **2011**, *133*, 9783.
[41] J. Kim, S. W. Lee, C. Carlton, S.-H. Yang, *J. Phys. Chem. Lett.* **2011**, *2*, 1332.
[42] S. Dong, X. Chen, L. Gu, X. Zhou, L. Li, Z. Liu, P. Han, H. Xu, J. Yao, H. Wang, X. Zhang, C. Shang, G. Cui, L. Chen, *Energy Environ. Sci.* **2011**, *4*, 3502.
[43] R. Liu, S. B. Lee, *J. Am. Chem. Soc.* **2008**, *130*, 2942.
[44] F.-F. Cao, Y.-G. Guo, S.-F. Zheng, X.-L. Wu, L.-Y. Jiang, R.-R. Bi, L.-J. Wan, J. Maier, *Chem. Mater.* **2010**, *22*, 1908.
[45] F.-F. Cao, Y.-G. Guo, L.-J. Wan, *Energy Environ. Sci.* **2011**, *4*, 1634.
[46] A. S. Arico, A. K. Shukla, H. Kim, S. Park, M. Min, V. Antonucci, *Appl. Surf. Sci.* **2001**, *172*, 33.
[47] F. Su, Z. Tian, C. K. Poh, Z. Wang, S. H. Lim, Z. L. Liu, J. Lin, *Chem. Mater.* **2010**, *22*, 832.
[48] A. S. Arico, A. Stassi, I. Gatto, G. Monforte, E. Passalacqua, V. Antonucci, *J. Phys. Chem. C* **2010**, *114*, 15823.
[49] D. Choi, P. N. Kumta, *J. Electrochem. Soc.* **2006**, *153*, A2298.
[50] J. Wang, G. Yin, Y. Shao, S. Zhang, Z. Wang, Y. Gao, *J. Power Sources* **2007**, *171*, 331.
[51] L. Li, X. Zhao, A. Manthiram, *Electrochem. Commun.* **2012**, *14*, 78.
[52] P. He, Y. Wang, H. Zhou, *Chem. Commun.* **2011**, *47*, 10701.

Received: April 24, 2012
Published online on August 3, 2012

